JOURNAL OF THERMOPHYSICS AND HEAT TRANSFER
Vol. 27, No. 1, January–March 2013

Temperature Stratification in a Cryogenic Fuel Tank

Matthew J. Daigle* and Vadim N. Smelyanskiy†
NASA Ames Research Center, Moffett Field, California 94035
and
Jacob Boschee‡ and Michael Foygel§
South Dakota School of Mines and Technology, Rapid City, South Dakota 57701

DOI: 10.2514/1.T3933

A reduced dynamic model describing temperature stratification effects driven by natural convection in a liquid hydrogen cryogenic fuel tank has been developed. It accounts for cryogenic propellant loading, storage, and unloading in the conditions of normal, increased, and microgravity. The model involves multiple horizontal control volumes in both liquid and ullage spaces. Temperature and velocity boundary layers at the tank walls are taken into account by using correlation relations. Heat exchange involving the tank wall is considered by means of the lumped-parameter method. By employing basic conservation laws, the model takes into consideration the major multiphase mass and energy exchange processes involved, such as condensation–evaporation of the hydrogen, as well as flows of hydrogen liquid and vapor in the presence of pressurizing helium gas. The model involves a liquid hydrogen feed line and a tank ullage vent valve for pressure control. The temperature stratification effects are investigated, including in the presence of vent valve oscillations. A simulation of temperature stratification effects in a generic cryogenic tank has been implemented in MATLAB and results are presented for various tank conditions.

Nomenclature

A	=	lateral surface of boundary layer element, m^2
$c_{P(V)}$	=	constant pressure (volume) specific heat, J/K · kg
f	=	dimensionless resistance coefficient
Gr, Nu, Ra, Re, Pr	=	dimensionless Grashof, Nusselt, Rayleigh, Reynolds, and Prandtl numbers, respectively
g	=	acceleration due to gravity, m/s^2
H	=	height of external tank, m
$H_{l(v)}$	=	height of liquid (vapor), m
h	=	specific enthalpy, J/kg
J	=	gas/vapor or liquid mass flow rate, kg/s
m	=	mass of a control volume, kg
p	=	(partial) pressure, Pa
$\dot{Q}$	=	heat flow rate from or to a control volume, W
$\dot{q}$	=	heat flow flux from or to a control volume, W/m^2
R	=	radius of external tank, storage tank, or a pipe, m
R_v, R_g	=	hydrogen and helium gas constants, J/(K · kg)
S	=	cross-sectional area of vent valve area, m^2
T	=	absolute temperature, K
t	=	time, s
u	=	specific internal energy, J/kg
V	=	volume, m^3
v	=	velocity of liquid or vapor, m/s
$\dot{W}$	=	power on or by a control volume, W
x	=	vertical position counted with respect to bottom of corresponding control volume, m
α	=	convection heat transfer coefficient, $W/(m^2 \cdot K)$
β	=	coefficient of volumetric expansion, 1/K
γ	=	ratio of specific heats, c_P/c_V
Δ	=	thickness of the horizontal layer, m
δ	=	thickness of boundary layer, m
κ	=	thermal conductivity, W/(m · K)
λ	=	dimensionless vent valve position
μ	=	dynamic viscosity, kg/(m · s)
ν	=	kinematic viscosity, m^2/s
ρ	=	density, kg/m^3

Subscripts

a	=	ambient
B	=	bulk-layer element
C	=	critical point
e	=	external heat or mass flows across the control volume boundaries other than liquid/vapor interface
f	=	gaseous hydrogen vapor film
g	=	gaseous helium
hor	=	horizontal surface
k	=	total number of liquid control volume layers
L	=	boundary-layer element
l	=	liquid hydrogen
lam	=	laminar flow
ls	=	saturated liquid
lv	=	liquid/vapor phase transition
n	=	total number of layers in vapor control volume
S	=	liquid/vapor interface
turb	=	turbulent flow
v	=	gaseous hydrogen vapor
vs	=	saturated vapor
w	=	tank wall

Superscripts

cond	=	conduction
conv	=	convection
λ	=	gaseous hydrogen or helium

Received 9 April 2012; revision received 4 September 2012; accepted for publication 5 September 2012; published online 29 November 2012.

*Research Computer Scientist, Intelligent Systems Division.
†Senior Research Scientist, Applied Physics Group Lead.
‡Graduate Student, Physics Department.
§Professor, Physics Department.

I. Introduction

RECENTLY, a dynamic model was developed for a complex spatially distributed system of liquid hydrogen (LH2) loading that involves the storage (ST) and external (ET) tanks as well as the

transfer line [1]. This reduced model is based on a set of coupled ordinary integro-differential equations, which is shown to be well suited to describing a generic cryogenic loading system, including one used for space shuttle fueling in both the nominal and major faulty regimes. The model accounts for the pressurizing helium gas injected into the ET and can be easily modified for similar cryogenic propellant loading systems.

Analysis has been performed for both the nominal regime and the effects of several primary faults, such as gas leaks in the ullage space of both the ST and ET, as well as clogging of the ET vent valve on the history of both tanks [1,2]. It is found that each of the faults is characterized by quite a pronounced dynamics. The most interesting observation is that some of the faults, such as a substantial clogging of the ET vent valve, usually have a slight effect on the integral variables, namely on the volumes of LH2 in the tanks or even on the ullage temperatures and pressures. Yet, the dynamics of the ET vent valve switching that cause pressure oscillations are shown to be extremely sensitive even to small deviations from the nominal regime and can be used for early fault identification by means of real-time sensor data analysis. (The valve in question works between two threshold positions to maintain a required ullage pressure [1].) It means that one cannot only detect, isolate, and identify different faults based on the analysis of the sensor data characterizing the filling dynamics, but also infer the parameters of the model to be further used for prediction of future behavior of the system [2].

However, the preceding model, allowing for a fairly adequate description of the ET ullage history [1,2], does not account for a substantial temperature stratification that may happen [3–6] in both the ullage [7–10] and the liquid [9,10] control volumes of the external and storage cryogenic tanks. The major goal of the present paper is to develop a model that correctly describes possible thermal stratification in both the ullage and liquid bulk parts of a tank that is based on ordinary differential equations, similar to those discussed in [1], short of a full-scale computational fluid dynamics modeling scheme [3–8], so that it can be implemented efficiently and used for online state estimation, fault diagnosis, and fault prognosis. A distinctive feature of this model is that it takes into consideration nonequilibrium mass and energy exchange processes of condensation–evaporation at the liquid–vapor interface between the liquid and gas, and the thermal convection in both the liquid and vapor parts of the tank, which is driven by complex phenomena developing in the boundary layers adjacent to the tank walls as well as to the liquid–vapor interface.

The temperature stratification effects under consideration may be responsible for the possible appearance of the overheated layers [11,12] of cryogenic fuel in the external tanks and would be crucial to designing effective pressure and temperature control in the storage tanks [7–10,13]. The model is meant to be applied toward treating very important aspects of cryogenic fuel management technology [13], such as the minimization of the boil-off effects and the optimization of fuel bias, that is, of the excess of fuel load above nominal aimed at preventing the cryogenic fuel from overheating due to radiation from the hot jet and heat conduction transfer through the ET walls from the engine, thrust cone, and common bulkhead. The overheated cryogenic liquid on its way to the engine may reach a pump impeller, thus leading to the development of violent cavitation [14] in the areas where pressure is less than the saturated pressure of the overheated fuel.

The contributions of this work are as follows. We develop a general model of a cryogenic tank including temperature stratification effects in the liquid, vapor, and tank control volumes for an arbitrary number of lumped-parameter layers. We develop a simulation that implements the model and allows the investigation of the dynamic behavior under both storage, loading, and unloading regimes. In particular, we show that the presence of a vent valve in the tank used for the purposes of maintaining pressure creates temperature waves that propagate through the layers. Simulation results are presented and detailed analysis is provided.

The paper is organized as follows. Section II describes the cryogenic tank model, which incorporates temperature stratification effects driven by convection in both the liquid and vapor parts of the tank. Section III deals with major results of our simulations of the LH2 cryogenic tank in different performance regimes. Section IV concludes the paper.

II. Description of Model

Consider a cylindrical tank of radius R where the gravity/inertia force is parallel to its axis. It is partially filled with LH2; its ullage volume is filled by a mixture of gaseous hydrogen (GH2) and gaseous helium (GHe). The liquid and ullage (vapor) control volumes (CVs) are separated by a thin, massless film of saturated hydrogen [1] (see Fig. 1). The following subsections describe the liquid and vapor CVs and the heat and mass flows depicted in Fig. 1.

A. Vapor Control Volume

Divide the vapor (ullage) CV into $n \geq 3$ layers perpendicular to the axis of the tank. The lowest one ($i = 1$) is adjacent to the saturated film CV and exchanges mass and energy with it. The upper one ($i = n$) is at the top of the tank and exchanges heat with the top wall of the tank, as well as mass and energy with the environment through the vent valve, as shown in Fig. 1. Any internal horizontal slice ($i = 2, \ldots, n-1$), in turn, consists of two sub volumes: 1) a torus-shaped element of the boundary layer L, which is adjacent to the lateral wall of the tank and exchanges heat with it; and 2) the cylinder-shaped bulk element B, which is coaxial with the tank vertical axis x. Thus the total number of the vapor CVs is equal to $2(n-2)+2 = 2(n-1)$.

In the presence of the two gas components in the vapor CV GH2 v and GHe g, for the ith internal vapor bulk B element (see Fig. 1), the mass and the energy conservation, respectively, yield [15–21]

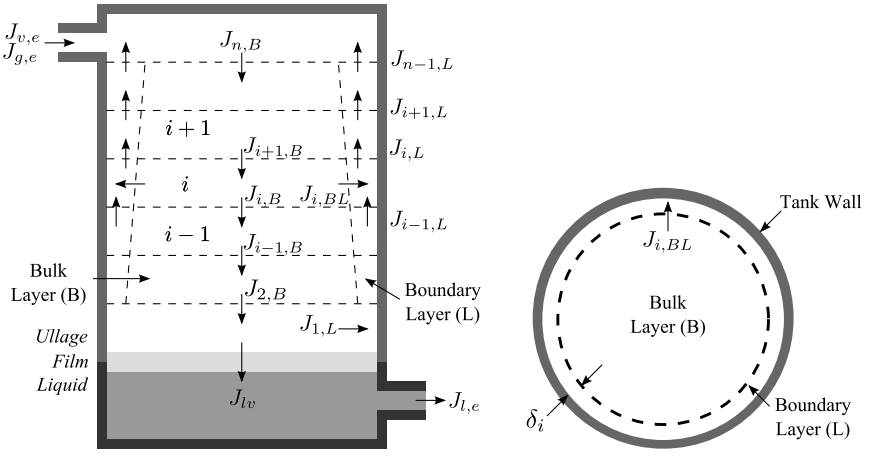

a) Side view **b) Top view**

Fig. 1 Mass flow in a propellant tank with three control volumes (vapor, film, and liquid).

$$\dot{m}^{(\lambda)}_{i,B} = J^{(\lambda)}_{i+1,B} - J^{(\lambda)}_{i,B} - J^{(\lambda)}_{i,BL} \tag{1}$$

$$\frac{\mathrm{d}}{\mathrm{d}t}\sum_{\lambda=v,g} m^{(\lambda)}_{i,B}u^{(\lambda)}_{i,B} = -\dot{W}^{(v)}_{i,B} + \sum_{\lambda=v,g} J^{(\lambda)}_{i+1,B}h^{(\lambda)}_{i+1,B} - (J^{(\lambda)}_{i,B} + J^{(\lambda)}_{i,BL})h^{(\lambda)}_{i,B} \tag{2}$$

where $\lambda = v, g$. Here, when the tank walls are hotter than the gas/vapor ($T_{wv} > T^{(v)}_{i,B}$), the flow vertically enters the element (i, B) from the preceding layer $(i + 1, B)$ and exits to an underlying bulk element $(i - 1, B)$; the remaining part (i, BL) spreads radially outward and enters the ith internal boundary-layer L element (see Fig. 1).

Similarly, for the ith internal boundary-layer L element (see Fig. 1)

$$\dot{m}^{(\lambda)}_{i,L} = J^{(\lambda)}_{i-1,L} - J^{(\lambda)}_{i,L} + J^{(\lambda)}_{i,BL} \tag{3}$$

$$\frac{\mathrm{d}}{\mathrm{d}t}\sum_{\lambda=v,g} m^{(\lambda)}_{i,L}u^{(\lambda)}_{i,L} = \dot{Q}^{(v)}_{i,e} - \dot{W}^{(v)}_{i,L} + \sum_{\lambda=v,g} J^{(\lambda)}_{i-1,L}h^{(\lambda)}_{i-1,L} - J^{(\lambda)}_{i,L}h^{(\lambda)}_{i,L} + J^{(\lambda)}_{i,BL}h^{(\lambda)}_{i,B} \tag{4}$$

Here, the specific enthalpies and energies of the elements are proportional to their absolute temperatures:

$$h^{v(g)}_{i,L(B)} = c_{P,v(g)}T_{i,L(B)} \tag{5}$$

$$u^{v(g)}_{i,L(B)} = c_{V,v(g)}T_{i,L(B)} \tag{6}$$

For the ith layer, the power associated with the change in its volume, $V_{i,B(L)}$ [1,15]

$$\dot{W}^{(v)}_{i,B(L)} = (p_v + p_g)\dot{V}^{(v)}_{i,B(L)} \tag{7}$$

The rate of the heat transfer from the wall to the vapor boundary-layer element [15–21]

$$\dot{Q}^{(v)}_{i,e} = \alpha_i A_i (T_{w,v} - T^{(v)}_{i,B}) \tag{8}$$

where $A_i = 2\pi R\Delta_i$ is the lateral surface of the boundary-layer element of the height Δ_i. (In this paper, the tank wall in contact with vapor is treated as a separate CV with temperature T_{wv} compared with the tank part in contact with LH2, which has temperature T_{wl}.)

In the case of the isothermal vertical wall (Fig. 2), the heat transfer coefficient can be calculated as [7,8,16–21]

$$\alpha_i = \frac{\kappa}{x_i}\begin{cases} 0.68 + 0.503(Ra_i\Psi)^{1/4}, & 10^5 < Ra < 10^9 \\ 0.15(Ra\Psi)^{1/3}, & 10^9 \le Ra < 10^{11} \end{cases} \tag{9}$$

where x_i is the average elevation of the ith layer counted from the interface (vapor film), κ is the thermal conductivity of the GH2/GHe mixture, and

$$\Psi = \left(1 + \left(\frac{0.492}{Pr}\right)^{9/16}\right)^{-16/9} \tag{10}$$

Here, the Raleigh number

$$Ra_i = Gr_i Pr \tag{11}$$

and the Grashof number

$$Gr_i = \frac{g\beta(T_w - T_{i,B})x_i^3}{\nu^2} \tag{12}$$

The Prandtl number $Pr = \mu c_P/\kappa$, where, for an ideal gas, the coefficient of the volumetric expansion $\beta = 1/T_{i,L}$.

The vertical mass flow rates within the ith boundary layer ($i = 1, \ldots, n - 1$) can be estimated as [7,8]

$$J_{i,L} = 2\pi R\rho_i v_i \delta_i \begin{cases} 0.0833, & \text{lam} \\ 0.1436, & \text{turb} \end{cases} \tag{13}$$

where the average velocity of the vertical boundary-layer flow [16–21]

$$v_i = 1.185\frac{\nu}{x_i}\left(\frac{Gr_i}{1 + 0.494Pr^{2/3}}\right)^{1/2} \tag{14}$$

and the thickness of the velocity boundary layer, within which the vertical component of the velocity is not very small (Fig. 2), can be calculated as [16–21]

$$\delta_i = x_i \begin{cases} 3.93\left(\frac{0.952+Pr}{Gr_i Pr^2}\right)^{1/4}, & \text{lam} \\ 0.565\left(\frac{1+0.494Pr^{2/3}}{Gr_i}\right)^{1/10}/Pr^{8/15}, & \text{turb} \end{cases} \tag{15}$$

It can be seen that the vertical mass flow rate is fully defined by the parameters of the corresponding boundary-layer element (i, L). In the case of natural convection, the mass flow is treated as laminar when the Raleigh number (11), which here plays a role of the Re number, is small [15], usually $Ra < 10^9$ [15–20]. The thickness of the thermal boundary layer, where the temperature changes from that of the wall T_w to that of the bulk $T_{i,L}$

$$\delta_{i,T} = \delta_i/Pr^{1/2} \tag{16}$$

is usually smaller than that of the velocity layer ($Pr > 1$) [16–20] (see Fig. 2). In this paper, the effects of film boiling are ignored [14]. A slight modification of the preceding formulas, describing the boundary-layer effects, is required if the wall is not considered isothermal (see [15–21] and Appendix A).

For the lowest horizontal vapor layer ($i = 1$), which is in contact with the film CV,

$$\dot{m}^{(v)}_{1,B} = J^{(v)}_{2,B} - J^{(v)}_{1,L} - J_{lv} \tag{17}$$

$$\dot{m}^{(g)}_{1,B} = J^{(g)}_{2,B} - J^{(g)}_{1,L} \tag{18}$$

$$\frac{\mathrm{d}}{\mathrm{d}t}\sum_{\lambda=v,g} m^{(\lambda)}_{1,B}u^{(\lambda)}_{1,B} = \dot{Q}_v - \dot{W}^{(v)}_{1,B} + \sum_{\lambda=v,g}(J^{(\lambda)}_{2,B}h^{(\lambda)}_{2,B} - J^{(\lambda)}_{1,L}h^{(\lambda)}_{1,L}) - J_{lv}h_{vs} \tag{19}$$

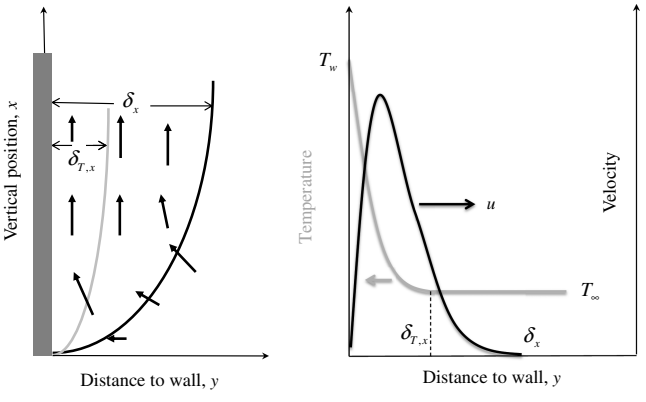

a) b)

Fig. 2 Natural convection from a vertical wall: a) boundary layer; b) temperature and velocity profiles.

Here, it is assumed that the lowest horizontal layer does not have the boundary element, so that the horizontal flow is equal to the upward vertical flow $(1, L)$ and is given by Eq. (13).

In accordance with [1], the rate of the heat exchange between the lowest horizontal gaseous layer and the vapor interface film CV (Fig. 3), which is driven either by convection or by conduction, can be calculated as

$$\dot{Q}_v = \pm \max\{\dot{Q}_v^{\text{cond}}, \dot{Q}_v^{\text{conv}}\} \tag{20}$$

where $+$ is chosen when the temperature of the vapor–liquid interface, $T_f = T_S < T_{1,B}^{(v)}$, and $-$ otherwise; the rate of the heat exchange due to convection

$$\dot{Q}_v^{\text{conv}} = \pi R^2 \alpha_{\text{hor}}^{(v)} (T_S - T_{1,B}^{(v)}) H(T_S - T_{1,B}^{(v)}) \tag{21}$$

where the Heaviside function H takes care of the proper temperature condition required for convection; the heat transfer coefficient from a horizontal surface [16–20]

$$\alpha_{\text{hor}} = \frac{\kappa}{R} \begin{cases} 0.54 Ra_R^{1/4}, & 10^4 < Ra_R < 10^7 \\ 0.15 Ra_R^{1/3}, & 10^7 \le Ra_R < 10^{11} \end{cases} \tag{22}$$

Here, the Ra_R number is given by Eqs. (11) and (12) where $T_w - T_{i,B}$ should be substituted with $T_s - T_{1,B}$ and x with R; and Ψ is given by Eq. (10). In Eq. (20), the rate of the heat exchange due to conduction $\dot{Q}_v^{\text{cond}}$ when it dominates heat flow through the interface, is defined by the time evolution of the temperature of the interface (film) $T_S(t)$. All the details of computation of $\dot{Q}_v^{\text{cond}}$ can be found in our previous paper [1].

For the upper horizontal layer (Fig. 3), which is in contact with the top of the tank and presumably with the vent valve,

$$\dot{m}_{n,B}^{(\lambda)} = J_{n-1,L} - J_{n,B}^{(\lambda)} + J_{\lambda,e} \tag{23}$$

$$\frac{\mathrm{d}}{\mathrm{d}t} \sum_{\lambda=v,g} m_{n,B}^{(\lambda)} u_{n,B}^{(\lambda)} = \dot{Q}_{\text{top}} - \dot{W}_{n,B}^{(v)} + \sum_{\lambda=v,g} (J_{n-1,L}^{(\lambda)} h_{n-1,L}^{(\lambda)} - J_{n,B}^{(\lambda)} h_{n,B}^{(\lambda)} + J_{\lambda,e}(h_{n,B}^{(\lambda)} + v_{\lambda,e}^2/2)) \tag{24}$$

where the rate of the heat exchange with the top of the tank is given by

$$\dot{Q}_{\text{top}} = \pi R^2 \alpha_{\text{hor}}^{(v)} (T_{wv} - T_{n,B}^{(v)}) \tag{25}$$

with the heat transfer coefficient given by Eq. (22) where $T_S - T_{1,B}$ should be substituted with $T_{wv} - T_{n,B}^{(v)}$. Here, it is assumed that the upper horizontal layer does not have the boundary element (see Fig. 1).

B. Liquid Control Volume

Divide the liquid CV into k horizontal layers, similar to the vapor CV. [The total number of the liquid CVs is equal to $2(k-1)$.] Then, for the jth bulk element $(j = 2, \ldots, k-1)$; the levels are counted from the bottom of the tank up to the liquid/vapor interface

$$\dot{m}_{j,B}^{(l)} = J_{j+1,B}^{(l)} - J_{j,B}^{(l)} - J_{j,BL}^{(l)} \tag{26}$$

$$\frac{\mathrm{d}}{\mathrm{d}t} m_{j,B}^{(l)} u_{j,B}^{(l)} = -\dot{W}_{j,B}^{(l)} + J_{j+1,B}^{(l)} h_{j+1,B}^{(l)} - (J_{j,B}^{(l)} + J_{j,BL}^{(l)}) h_{j,B}^{(l)} \tag{27}$$

For the jth internal boundary-layer L liquid element, the mass and energy conservation, respectively, yield (see Figs. 1 and 3)

$$\dot{m}_{j,L}^{(l)} = J_{j-1,L}^{(l)} - J_{j,L}^{(l)} + J_{j,BL}^{(l)} \tag{28}$$

$$\frac{\mathrm{d}}{\mathrm{d}t} m_{j,L}^{(l)} u_{j,L}^{(l)} = \dot{Q}_{j,e}^{(l)} - \dot{W}_{j,L}^{(l)} + J_{j-1,L}^{(l)} h_{j-1,L}^{(l)} - J_{j,L}^{(l)} h_{j,L}^{(l)} + J_{j,BL}^{(l)} h_{j,B}^{(l)} \tag{29}$$

Here, the specific enthalpy and energy are close to each other and both approximately equal to [1]

$$h_{j,L(B)} \approx u_{j,L(B)} \approx c_l T_{j,L(B)} \tag{30}$$

For the upper horizontal layer, which is in contact with the film CV (interface),

$$\dot{m}_{k,B}^{(l)} = -J_{k,B}^{(l)} + J_{k-1,L}^{(l)} + J_{lv} \tag{31}$$

$$\frac{\mathrm{d}}{\mathrm{d}t} m_{k,B}^{(l)} u_{k,b}^{(l)} = \dot{Q}_l - \dot{W}_{k,B}^{(l)} - J_{k,B}^{(l)} h_{k,b}^{(l)} + J_{k-1,L}^{(l)} h_{k-1,L}^{(l)} + J_{lv} h_{ls} \tag{32}$$

Here, it is assumed that the lowest horizontal layer does not have the boundary element, so that the upward vertical flow is equal to the horizontal flow and is given by Eq. (13).

Here, the rate of the heat exchange with the film CV

$$\dot{Q}_l = \pm \max\{\dot{Q}_l^{\text{cond}}, \dot{Q}_l^{\text{conv}}\} \tag{33}$$

where $+$ is chosen when $T_S > T_{k,B}^{(l)}$, and $-$ otherwise; the rate of the heat exchange due to convection

$$\dot{Q}_l^{\text{conv}} = \pi R^2 \alpha_{\text{hor}}^{(l)} (T_{k,B}^{(l)} - T_S) H(T_{k,B}^{(l)} - T_S) \tag{34}$$

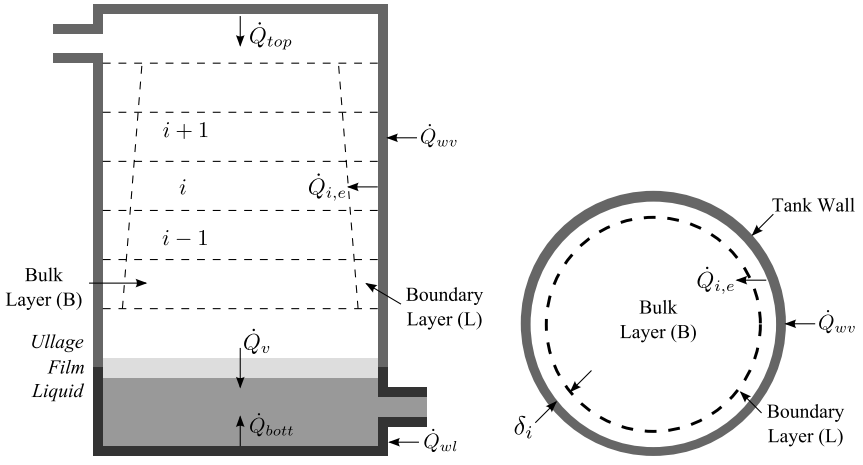

a) Side view **b) Top view**

Fig. 3 Heat flow in a propellant tank with three control volumes (vapor, film, and liquid).

with the heat transfer coefficient given by Eq. (22) with parameters corresponding to LH2 [15–21].

For the lowest horizontal layer, which is in contact with the bottom of the tank, and, assumed to be with a transfer line valve,

$$\dot{m}^{(l)}_{1,B} = -J^{(l)}_{1,B} + J^{(l)}_{2,B} - J_{l,e} \tag{35}$$

$$\frac{\mathrm{d}}{\mathrm{d}t} m^{(l)}_{1,B} u^{(l)}_{1,B} = \dot{Q}_{\mathrm{bott}} - \dot{W}^{(l)}_{1,B} - J^{(l)}_{1,B} h^{(l)}_{1,B} + J^{(l)}_{2,L} h^{(l)}_{2,L} - J_{l,e}(h^{(l)}_{1,B} + v^2_{l,e}/2) \tag{36}$$

where the rate of the heat exchange with the bottom

$$\dot{Q}_{\mathrm{bott}} = \pi R^2 \alpha^{(l)}_{\mathrm{hor}} (T_{wl} - T^{(l)}_{1,B}) \tag{37}$$

with the heat transfer coefficient given by Eq. (22) where $T_{wv} - T^{(v)}_{1,B}$ should be substituted with $T_{wl} - T^{(l)}_{1,B}$. Here, it is assumed that the lowest liquid horizontal layer does not have the boundary element. (All the details of computation of the heat flow due to conduction $\dot{Q}^{\mathrm{cond}}_l$ can be found in our previous paper [1].)

C. Summary of Model

Thus, dividing the liquid CV into k horizontal layers and the vapor CV into n layers, one deals with the following $2(5n + 3k) - 13$ state variables: $4(n-1) + 2(k-1) = 2(2n + k - 3)$ masses $m^{(\lambda)}_{1,B}, m^{(\lambda)}_{n,B}, m^{(\lambda)}_{i,B(L)}, m^{(l)}_{1,B}, m^{(l)}_{k,B}, m^{(l)}_{j,B(L)}$ $(i = 2, \ldots, n-1;\ j = 2, \ldots, k-1;\ \lambda = v, g)$; vapor CV partial pressures and volume p_v, p_g and V_v; $2(n + k) - 1$ temperatures $T_f, T_{wl}, T_{wv}, T^{(v)}_{1,B}, T^{(v)}_{n,B}, T^{(v)}_{i,B(L)}, T^{(l)}_{1,B}, T^{(l)}_{k,B}, T^{(l)}_{j,B(L)}$ $(i = 2, \ldots, n-1;\ j = 2, \ldots, k-1$; and $4(n-2) + 2(k-2) + 3 = 2(2n + k) - 9$ mass flow rates $J^{(\lambda)}_{i,B}, J^{(\lambda)}_{i,BL}, J^{(\lambda)}_{n,B}, J^{(l)}_{j,B}, J^{(l)}_{j,BL}, J^{(l)}_{1,B}$ $(i = 2, \ldots, n-1;\ j = 2, \ldots, k-1;\ \lambda = v, g)$.

There are $4n + 2k - 5$ constraints: $4(n-1)$ GH2 and GHe equations of state

$$p_\lambda V^{(v)}_{i,B(L)} = m^{(\lambda)}_{i,B(L)} R_\lambda T^{(v)}_{i,B(L)} \tag{38}$$

where $\lambda = v, g$; the film equation of state

$$p_v = p_f(T_f) = p_C (T_f/T_C)^n \tag{39}$$

with $p_C = 1.315$ MPa and $T_C = 33.2$ K and $n = 5$ being, respectively, critical pressure and temperature for hydrogen [1] [in Eq. (38), the partial pressures are considered uniform across the vapor CV, with the LH2 partial pressure equal to that of the saturated vapor film Eq. (39)]; $2(k-1) - 1$ equations relating the liquid masses and volumes [because one liquid mass is fully defined by the total liquid mass, which, in turn is defined by (41)]

$$m^{(l)}_{j,L(B)} = \rho_l V^{(l)}_{j,L(B)} \tag{40}$$

and an equation that relates the total tank volume to the GH2 volume and LH2 volume

$$V = V_v + V_l = \left(V^{(v)}_{1,B} + V^{(v)}_{n,B} + \sum_{i=2}^{n-1} (V^{(v)}_{i,B} + V^{(v)}_{i,L})\right) + \left(V^{(l)}_{1,B} + V^{(l)}_{k,B} + \sum_{j=2}^{k-1} (V^{(l)}_{j,B} + V^{(l)}_{j,L})\right) \tag{41}$$

There are $6n + 4k - 4$ ordinary differential rate equations for $2(5n + 3k) - 13 - (4n + 2k - 9) = 6n + 4k - 4$ independent variables: $4(n-1)$ GH2 and GHe mass conservation Eqs. (1), (3), (17), (18), and (23); $4(n-1)$ GH2 and GHe energy conservation Eqs. (2), (4), (19), and (24); $2(k-1)$ LH2 mass conservation Eqs. (26), (28), (31), and (35); $2(k-1)$ LH2 energy conservation Eqs. (27), (29), (32), and (36); and two energy conservation equations for the two control volumes for the tank wall in contact with LH2 and the ullage, respectively (Fig. 3)

$$c_w d(m_{wl} T_{wl})/\mathrm{d}t = \begin{cases} \dot{Q}_{wl} - \dot{Q}^{(l)}_e + c_w \dot{m}_{wl} T_{wl}, & \dot{m}_{wl} < 0 \\ \dot{Q}_{wl} - \dot{Q}^{(l)}_e + c_w \dot{m}_{wl} T_{wv}, & \dot{m}_{wl} \geq 0 \end{cases} \tag{42}$$

$$c_w d(m_{wv} T_{wv})/\mathrm{d}t = \begin{cases} \dot{Q}_{wv} - \dot{Q}^{(v)}_e + c_w \dot{m}_{wv} T_{wl}, & \dot{m}_{wl} < 0 \\ \dot{Q}_{wv} - \dot{Q}^{(v)}_e + c_w \dot{m}_{wv} T_{wv}, & \dot{m}_{wl} \geq 0 \end{cases} \tag{43}$$

Here, the last terms in the right sides of Eqs. (42) and (43) describe the flow of internal energy along the tank walls due to motion of the liquid level and of the subsequent plane separating the two tank CVs (note that $\dot{m}_{wl} = -\dot{m}_{wv}$). Also, in the preceding equations, we ignore the direct heat exchange (due to conduction) between the two parts of the tank because the corresponding thermal length even for $t = 10^3$ s is shown to be much smaller than the size of those parts. The total heat transfer from the tank wall to the vapor CV [see Eqs. (8) and (25), Fig. 3]

$$\dot{Q}^{(v)}_e = \dot{Q}_{\mathrm{top}} + \sum_{i=2}^{n-2} \dot{Q}^{(v)}_{i,e} \tag{44}$$

and the total heat transfer from the tank wall to the liquid CV

$$\dot{Q}^{(l)}_e = \dot{Q}_{\mathrm{bott}} + \sum_{j=2}^{k-2} \dot{Q}^{(l)}_{j,e} \tag{45}$$

where

$$\dot{Q}^{(l)}_{j,e} = \alpha_j A_j (T_{wl} - T^{(l)}_{j,B}) \tag{46}$$

and $\dot{Q}_{\mathrm{bott}}$ is given by Eq. (37). Here, the heat transfer coefficients α_j are given by Eq. (8) with the parameters of liquid, and $A_j = 2\pi R \Delta_j$ is the lateral surface of the boundary-layer element of the height Δ_j.

And, finally, the condensation–evaporation mass flow rate through the LH2/GH2 interface J_{lv} is related to the heat flows through the same interface, $\dot{Q}_v$ Eq. (20) and $\dot{Q}_l$ Eq. (33) by means of the energy conservation equation for the film CV. Ignoring the film mass, it can be written as

$$\dot{Q}_v - \dot{Q}_l + J_{lv}(h_{vs} - h_{ls}) = \frac{\mathrm{d}}{\mathrm{d}t} m_f u_f = 0 \tag{47}$$

where the specific enthalpies are referred to those of the saturated vapor and liquid. The temperatures of the vapor liquid interface T_S is considered to be equal to that of the film T_f [1].

III. Results

The previously described model of temperature stratification has been explored in an LH2 tank. The parameter values of the cylindrical tank were chosen similar to that of the space shuttle ET [1,2], provided in Appendix C. In Eqs. (42) and (43), the material parameters of the tank are chosen to that typical for aluminum (see Table C1 in Appendix C). The tank is considered to be initially (at $t = 0$) half-filled with LH2: $V_l(0) = V/2$ with GH2 and GHe partial pressures $p_v(0) = p_g(0) = 1$ atm and initial temperatures of GH2/GHe mixture, LH2, and the tank, respectively, equal to $T_v(0) = T_l(0) = 20$ K and $T_w(0) = 21$ K. In addition, the tank absorbs heat from the environment [see Eqs. (42) and (43)] at a rate of $\dot{Q}_w = 20$ kW in the blowdown regime. Throughout modeling, the number of horizontal layers in the liquid CV was set equal to that in the vapor CV, where $n = k = 10$, which yields 146 state variables and 95 ordinary differential equations. It is found that starting from $n = k = 10$ and on, such "integral" characteristics as the total ullage pressure $p_v + p_g$ and the tank wall temperatures T_{wl} and T_{wv} converge and change no more than, respectively, 0.1 and 0.3% with the increase of the number of the horizontal layers. Those numbers can be taken as a measure of the uncertainty of the predicted results.

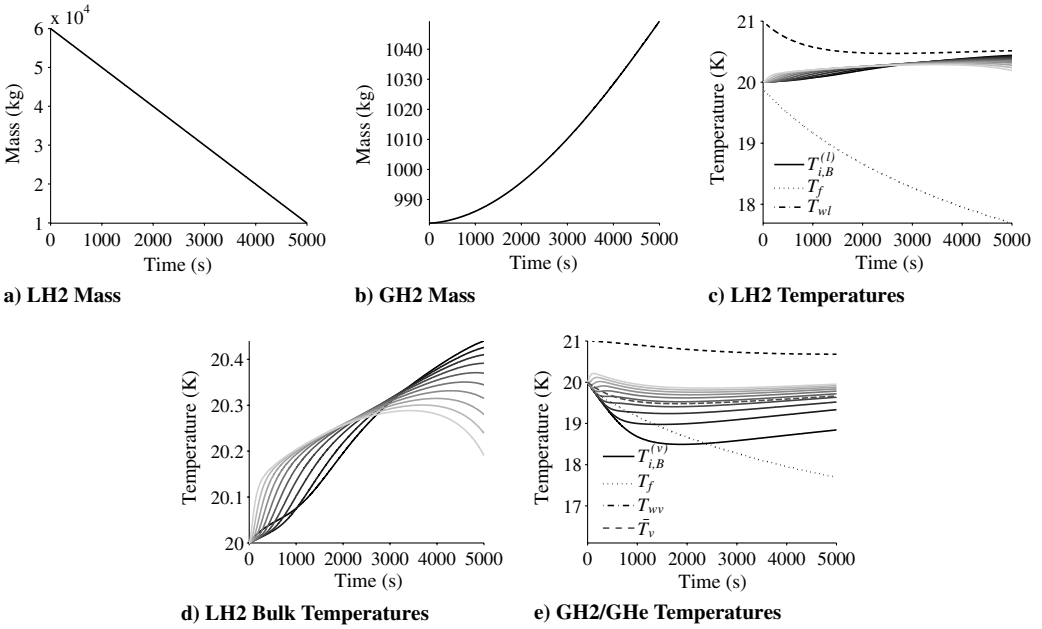

a) LH2 Mass b) GH2 Mass c) LH2 Temperatures

d) LH2 Bulk Temperatures e) GH2/GHe Temperatures

Fig. 4 Tank in a blowdown regime at normal gravity.

A. Blowdown Regime

In the blowdown regime, it is assumed that the ullage vent valve is closed ($J_{v,e} = J_{g,e} = 0$), and LH2 is being removed from the tank at a constant rate of $J_{l,e} = 10$ kg/s. The case of normal gravity is considered first. Figure 4 shows the masses and temperatures. (For this and all the subsequent figures, higher layers are shown with lighter-colored lines.) LH2 mass (Fig. 4a) drops, due to the positive external mass flow, but also due to evaporation, whereas the GH2 mass (Fig. 4b) increases due to evaporation. The very same evaporation is responsible for cooling off the LH2/GH2 interface, and the liquid–vapor interface temperature $T_S = T_f$ drops due to the evaporation (Figs. 4c and 4e). The lumped-parameter ullage temperature is also shown in Fig. 4e as $\bar{T}_v$ to demonstrate that the stratified temperatures behavior is consistent with the lumped-parameter formulation (see Appendix B). The expansion of the ullage volume leads to its initial cooling, which gives way to the subsequent ullage heating due to effective convection-assisted heat transfer from the tank wall (Fig. 4e). The temperatures of the liquid layers also increase due to heat transfer from the tank wall, as shown in Fig. 4c. Figure 4d shows only the temperatures of the liquid bulk temperatures, because the stratification is not easily observed in Fig. 4c. Figure 5 uses a heat map to show a visualization of temperature stratification, in this case, at different time instants.

Figure 6 demonstrates temperature evolution of different layers of the tank as it would be measured by sensors at fixed heights in the tank. Here, $n = 100$ is used to minimize an artificial "ripple" effect caused by transition from one layer to another, which happens at a fixed sensor height. It can be seen that, as the liquid level crosses the sensor at 12 m, the temperature experiences a sudden drop from the LH2 temperature to that of the GH2/GHe mixture. A small peak seen at the ullage temperature curves can be attributed to transient effects that develop at the early stages of the system evolution.

Figure 7 shows the masses and temperatures for the blowdown regime in elevated gravity ($7g$). Here, the evaporation rate is somewhat larger than the case of normal gravity (compare Figs. 4b and 7b), and stratification seems to be reduced slightly due to the enhanced convection-driven heat exchange between the tank body and its contents (see Figs. 7c, 7d and 7e). Figure 8 shows the visualization of temperature stratification in this case.

Figure 9 shows behavior of the masses and temperatures for the tank at the conditions of microgravity ($10^{-6}g$). Here, the heat

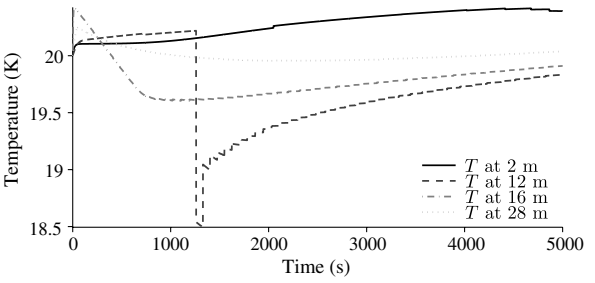

Fig. 6 Temperatures at fixed heights in a tank in a blowdown regime at normal gravity.

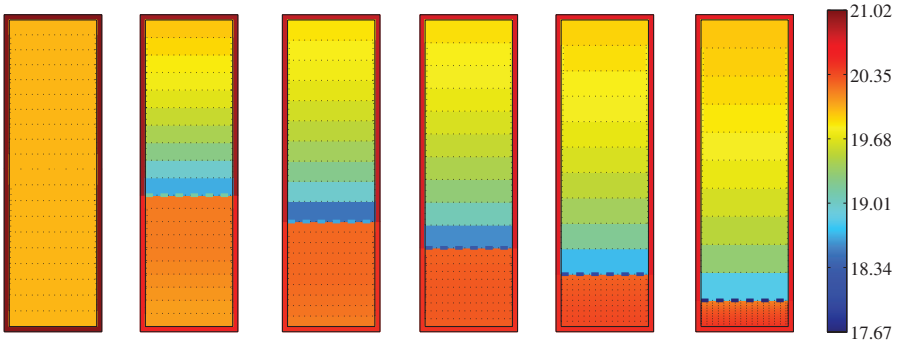

a) t = 0 s b) t = 1000 s c) t = 2000 s d) t = 3000 s e) t = 4000 s f) t = 5000 s

Fig. 5 Tank in a blowdown regime at normal gravity: temperature stratification.

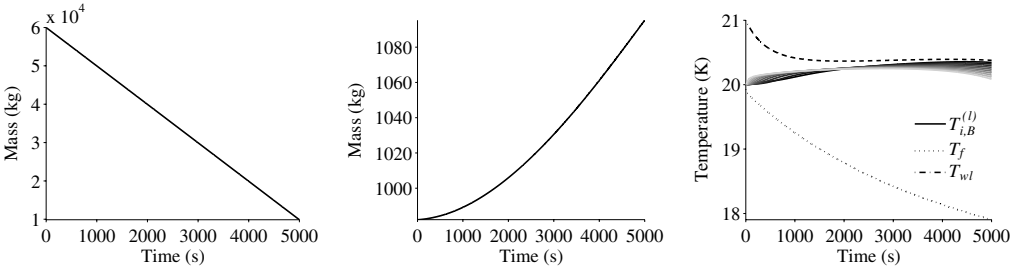

a) LH2 Mass b) GH2 Mass c) LH2 Temperatures

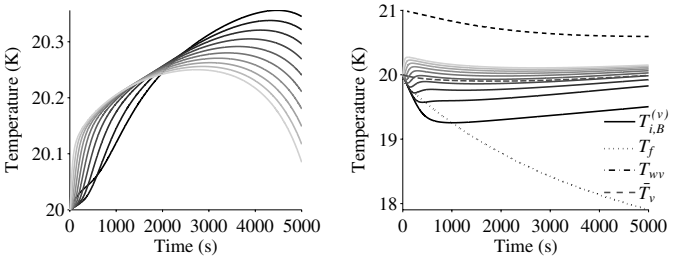

d) LH2 Bulk Temperatures e) GH2/GHe Temperatures

Fig. 7 Tank in a blowdown regime at elevated gravity 7*g*.

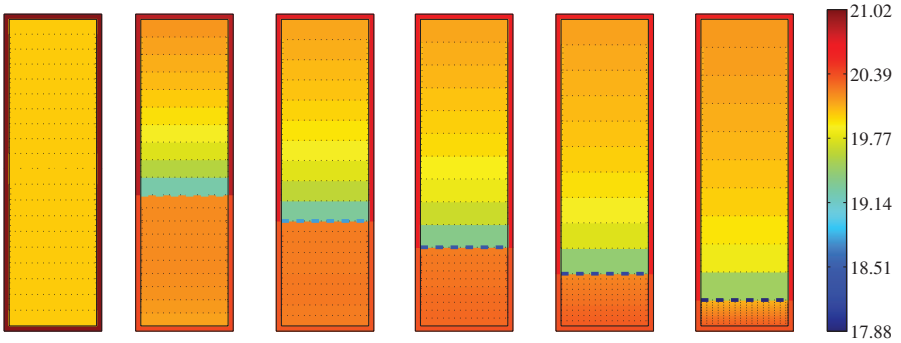

a) $t = 0$ s b) $t = 1000$ s c) $t = 2000$ s d) $t = 3000$ s e) $t = 3000$ s f) $t = 5000$ s

Fig. 8 Tank in a blowdown regime at elevated gravity: temperature stratification.

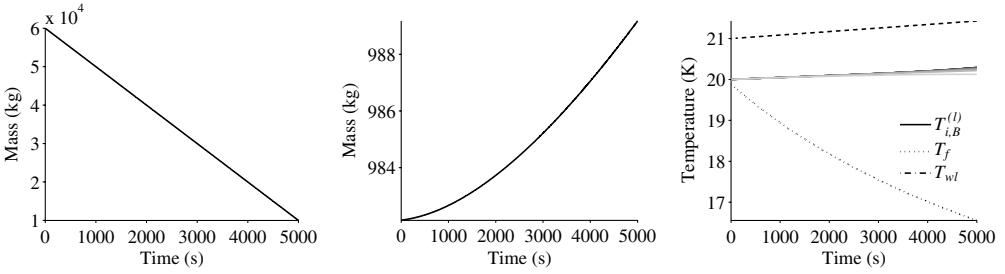

a) LH2 Mass b) GH2 Mass c) LH2 Temperatures

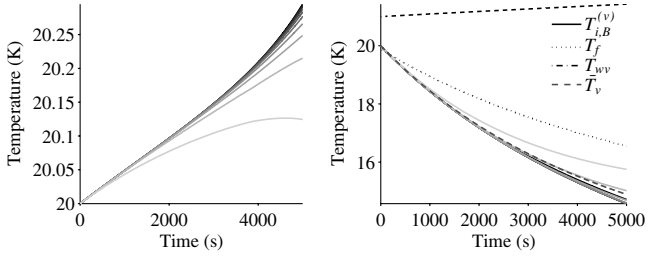

d) LH2 Bulk Temperatures e) GH2/GHe Temperatures

Fig. 9 Tank in a blowdown regime at microgravity.

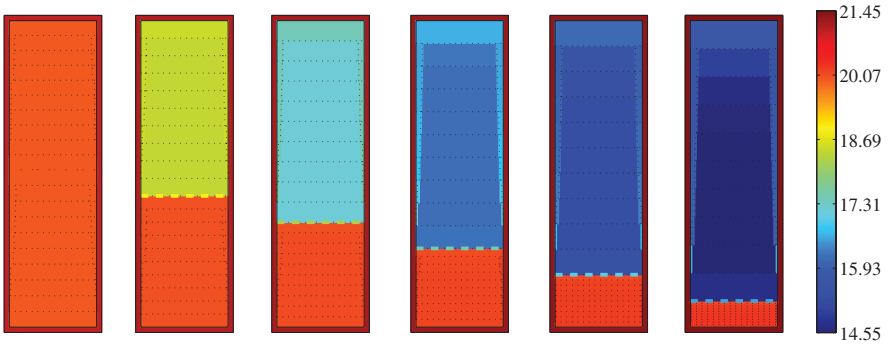

a) $t = 0$ s b) $t = 1000$ s c) $t = 2000$ s d) $t = 3000$ s e) $t = 4000$ s f) $t = 5000$ s

Fig. 10 Tank in a blowdown regime at microgravity: temperature stratification. (A slow development of the boundary layer can be seen at $t > 4000$ s.)

exchange between the tank wall and its contents is suppressed, thus leading to continuous cooling of the ullage due to its expansion. In this case, the suppression of the heat exchange, in contrast to the initial drop in the tank's temperature T_{wl} and T_{wv} at normal (Fig. 4) and elevated gravity (Fig. 7), causes continuous heating of the tank wall and diminishes temperature stratification effects in both the liquid and vapor CVs. This is clearly shown visualization of the temperature stratification in Fig. 10.

It should be mentioned here that, in all cases, as expected, the temperature stratification is much more pronounced in the ullage CV compared with the liquid CV due to much more effective convection flow and thermal conductivity in the LH2 ($J_L = 5$ kg/s in comparison with GH2/GHe where $J_L = 0.9$ kg/s). Figures 4e, 7e and 9e also demonstrate that the results of the simulations, which take into consideration the effects of temperature stratification, are fully consistent with previous ones (seen on T_v curves) that are obtained in the framework of the lumped-parameter method (see [1,2] and Appendix B).

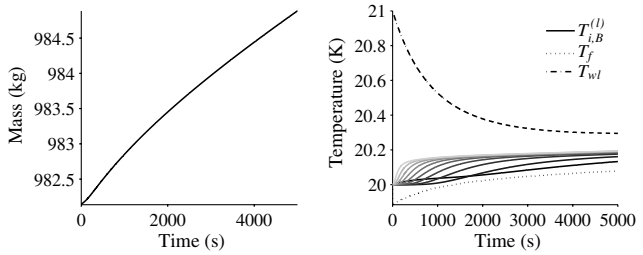

a) GH2 Mass

b) LH2 Temperatures

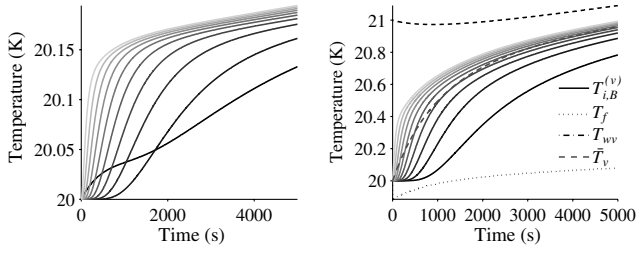

c) LH2 Bulk Temperatures

d) GH2/GHe Temperatures

Fig. 11 Tank in a storage regime at normal gravity without venting.

B. Storage Regime

The storage regime is now considered, where liquid is not added or removed from the tank ($J_{l,e} = 0$). The tank, with initial temperature set at $T_w(0) = 20.3$ K, is absorbing heat at a rate of $\dot{Q}_w = 10$ kW, which, for the tank of a chosen size, roughly corresponds to the radiation heat flux from the sun. Figure 11 demonstrates temperature evolutions in the unvented tank ($J_{v,e} = J_{g,e} = 0$) at the conditions of normal gravity. Here, evaporation is greatly reduced (Fig. 11a). Substantial temperature stratification in the ullage volume can be observed. Also, it can be seen that, in contrast to the blowdown regime (Fig. 4), all temperatures including that of the LH2/LG2 interface T_f rise because of continuing heat absorption. Here, again, the interface temperature is less than that of LH2 due to evaporation. The temperature stratification visualization is shown in Fig. 12. Everything starts out very cold, and temperature stratification occurs naturally as heat is added to the tank wall. The ullage heats up, whereas the liquid, due to its greater heat capacitance, stays relatively cool.

Introduction of a vent valve in the upper part of the ullage volume dramatically changes the picture, as shown in Fig. 13. The valve is set to operate between lower and upper thresholds at 2.002.00 and 2.02 atm, correspondingly. When the upper threshold is reached, the valve opens; it closes as soon as the lower limit is achieved. The gas flow rate through the vent valve $J_{v(g),e} = -J_{\text{valve}}^{v(g)}$ where, for the choked flow regime [22],

$$J_{\text{valve}}^{v(g)} = \lambda \rho_{v(g)} S_{v,\text{valve}} \sqrt{\frac{\gamma(p_v + p_g)}{\rho_v + \rho_g} \left(\frac{2}{\gamma + 1}\right)^{\frac{\gamma+1}{\gamma-1}}} \tag{48}$$

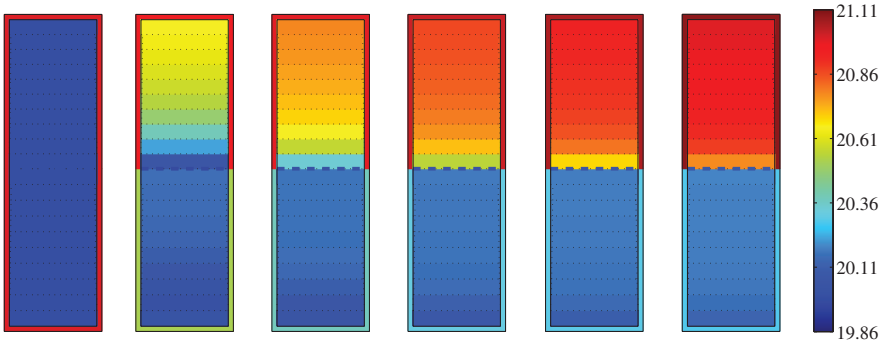

a) $t = 0$ s b) $t = 1000$ s c) $t = 2000$ s d) $t = 3000$ s e) $t = 4000$ s f) $t = 5000$ s

Fig. 12 Tank in a storage regime without venting at normal gravity: temperature stratification.

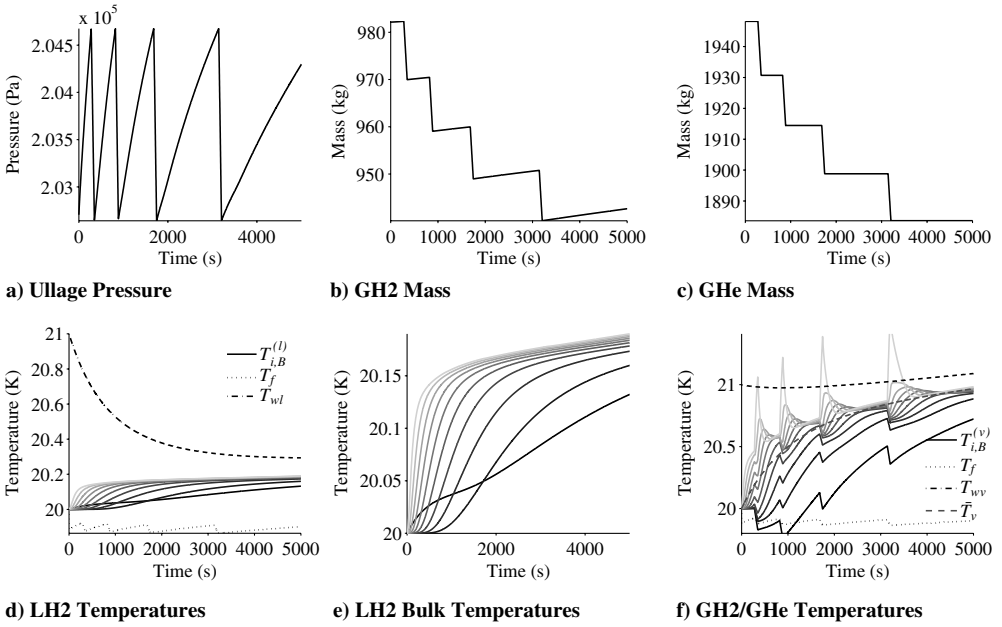

a) Ullage Pressure **b) GH2 Mass** **c) GHe Mass**

d) LH2 Temperatures **e) LH2 Bulk Temperatures** **f) GH2/GHe Temperatures**

Fig. 13 Tank in a storage regime at normal gravity with venting.

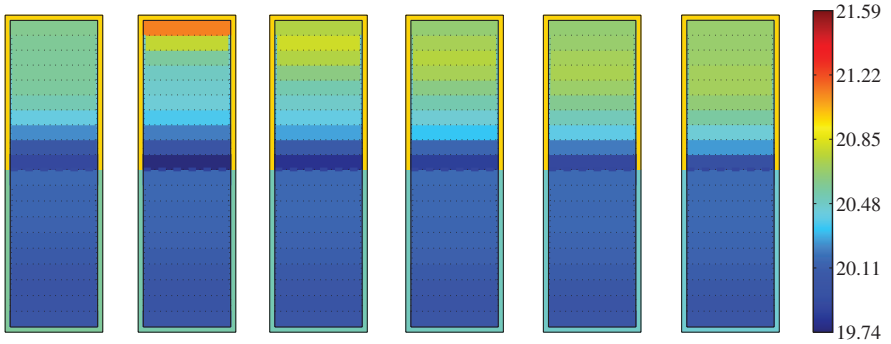

a) t = 800 s **b) t = 900 s** **c) t = 1000 s** **d) t = 1100 s** **e) t = 1200 s** **f) t = 1300 s**

Fig. 14 Tank in a storage regime with venting at normal gravity: temperature stratification.

Here, λ is a dimensionless relative valve position that assumes values between zero and one. For a given composition of the GH2/GHe mixture, parameter $\gamma = 1.51$, and the conditions for the choked flow regime [22] are satisfied. Also, in the present modeling, the valve's cross section area is set as $S_{\text{valve}} = 5$ cm^2. Each time the valve opens, a certain amount of the gas/vapor mixture from the upper layer is removed (Figs. 13b and 13c). Because that amount is small compared with the total ullage mass, its removal does not substantially change the ullage pressure (Fig. 13a), which is uniform across the ullage volume and propagates very quickly (with the speed of sound). Yet the removed mass is comparable with that of the upper layer, where mass reduction, in accordance with the equation of state (38), leads to a temperature spike (Fig. 13f). A subsequent temperature wave can be observed propagating in the downward direction due to downward convection circulation in the bulk layers (visualized in Fig. 14), which diminishes in intensity as it travels downward. As a result, on average, the temperatures rise at a smaller rate compared with the nonvent case (Fig. 12), and the interface temperature is being stabilized (Fig. 13f). Note that, due to fast propagation of the pressure, the temperature variations in the lower layers follow that of pressure and are opposite in phase to those of the upper layers.

IV. Conclusions

In the present paper, the dynamic model of a cryogenic fuel tank has been presented that incorporates effects of 1) temperature stratification driven by the natural convection in both the liquid and ullage control volumes and 2) highly nonequilibrium condensation–evaporation phenomena at the interface between those volumes. Unlike a standard full-scale computational fluid dynamics approach dealing with numerical solution of equations in partial derivatives, the proposed low-dimensional scheme reduces modeling to solution of a set of ordinary differential equations that account for basic conservation laws applied to the properly chosen control volumes. Those equations are demonstrated to successfully describe complex temperature stratification effects for different modes of the liquid hydrogen fuel tank operation.

First, it has been shown that the preceding effects are consistent with the description of the system in the framework of the lumped-parameter method. Second, time evolution of the temperature data collected by the fixed-elevation sensors can be described and analyzed in the framework of the developed approach. Third, complex effects such as temperature waves caused by a vent valve operating between given pressure thresholds can be found and understood by means of the simplified computational approach. Fourth, practically important and theoretically complex effects of normal, elevated, and microgravity can be taken into consideration, including their role in the heat exchange between the tank walls and the cryogenic fuel content. In particular, it has been demonstrated that the increased (decreased) gravity will substantially promote (suppress) such an exchange.

Appendix A: Uniform Heat Flux

In the preceding consideration, it is assumed that the tank is described by the uniform temperature of its body T_w. In the case of the

Table C1 Parameter values

Component	Parameter values
Hydrogen and helium	$T_c = 33.2$ K, $p_c = 1.315 \times 10^6$ Pa, $\lambda = 5$, $\rho_L = 71.1$ kg/m^3, $c_L = 9450$ J/(kg · K), $\kappa_L = 0.0984$ W/(m · K), $\mu = 3.4 \times 10^{-6}$ Pa s, $R_v = 4124$ J/(kg · K), $c_{V,v} = 6490$ J/(kg · K), $\gamma = 5/3$, $\kappa_v = 0.0166$ W/(m · K), $R_g = 2077$ J/(kg · K), $\kappa_g = 0.0262$ W/(m · K), $c_{V,g} = 3121$ J/(kg · K), $c_{P,g} = 5193$ J/(kg · K)
Tank	$n = k = 10$, $R = 4.21$ m, $H = 29.56$ m^2, $c_w = 1 \times 5 \times 10^2$ J/K, $\rho_w = 2700$ kg/m^3, $d_w = 0.1$ m, $S_{\text{valve}} = 0.05$ cm^2

uniform heat flux ($\dot{q}_w = \text{const}$), the local (average) Raleigh numbers Ra_x (Ra_H) that define the heat transfer coefficients (9) and (22) as well as the velocity Eq. (14) in, and the thickness Eq. (15) of, the boundary layers [via the Grashof numbers Eq. (12)], must be substituted by a modified Raleigh number [15]. It can be found by expressing Ra in terms of $\dot{q}_w$ by eliminating $T_w - T_{v(l)}$:

$$Ra_x^* = Ra_x Nu_x = \frac{g\rho^2 c_P \beta \dot{q}_w x^4}{\mu\kappa^2} \tag{A1}$$

so that the heat transfer coefficients in Eq. (9) are to be substituted with, correspondingly, the modified heat transfer coefficients [15]

$$\alpha_i = \frac{\kappa}{x_i} Nu_i = \frac{\kappa}{x_i} \begin{cases} 0.631(Ra_x^* \Psi)^{1/5}, & 10^5 < Ra_x^* < 10^9 \\ 0.241(Ra_x^* \Psi)^{1/4}, & 10^9 \le Ra_x^* < 10^{11} \end{cases} \tag{A2}$$

and

$$\bar{\alpha}_L = \frac{\kappa}{H_l} Nu_H = \frac{\kappa}{H_l} \begin{cases} 0.726(Ra_H^* \Psi)^{1/5}, & 10^5 < Ra_H^* < 10^9 \\ 0.241(Ra_H^* \Psi)^{1/4}, & 10^9 \le Ra_H^* < 10^{11} \end{cases} \tag{A3}$$

where Ψ is given by Eq. (10). Given the uniform heat flux $\dot{q}_w$, the local temperature at the wall surface can be found from

$$T_w = T_{v(l)} + \frac{\dot{q}_w}{\alpha} = T_{v(l)} + \frac{\dot{q}_w x}{Nu_x \kappa} \tag{A4}$$

where the Nu_x number can be found from Eq. (A2).

Appendix B: Lumped-Parameter Approximation

Here is described the lumped-parameter approximation for each of the three CVs: liquid, vapor, and film, similar to that presented in [1] by ascribing a common temperature to each of those CVs. In that case, the mass conservation equation for (e.g., the liquid CV) can be obtained by summing up Eqs. (26), (28), (31), and (35) over all liquid elements, thus yielding

$$\dot{m}_l = J_{lv} - J_{l,e} \tag{B1}$$

Here, the interface flow rate J_{lv} can be found by solving (7.1) together with the total mass conservation for the vapor CV

$$\dot{m}_v = -J_{lv} + J_{v,e} \tag{B2}$$

$$\dot{m}_g = J_{g,e} \tag{B3}$$

and the energy conservation for the liquid, vapor, and film CVs [see also Eq. (47)], all of which can be obtained in a similar way:

$$\dot{Q}_{l,e} + \dot{Q}_l + \dot{W} + J_{lv} h_{ls} + J_{l,e}(h_l + v_{l,e}^2/2) = \frac{\mathrm{d}}{\mathrm{d}t} m_l u_l \tag{B4}$$

$$\dot{Q}_{v,e} - \dot{Q}_v - \dot{W} - J_{lv} h_{vs} + J_{v,e}(h_v v_{v,e}^2/2) + J_{g,e}(h_g + v_{g,e}^2/2) = \frac{\mathrm{d}}{\mathrm{d}t}(m_v u_v + m_g u_g) \tag{B5}$$

complemented with the expression relating the liquid and vapor volumes

$$V = V_v + V_l = V_v + m_l/\rho_l \tag{B6}$$

and the film Eq. (39) and vapor (gas) equations of state

$$p_{v(g)} = \rho_{v(g)} R_{v(g)} T_v \tag{B7}$$

Given the external mass flow rates $J_{v,e}$, $J_{l,e}$ Eqs. (39), (47), and (B1–B7) allow one to find the rate of the total mass change $\dot{m}_l$ (or $\dot{V}_l$) for the liquid CV, the rate of the volume change $\dot{V}_v$ of the vapor CV, as well as the "average" temperatures T_l, T_v as functions of time. In this step, the local convection heat transfer coefficients for the vertical surfaces should be substituted by their average values [15]

$$\bar{\alpha}_H = \frac{\kappa}{H_{l(v)}} \begin{cases} 0.68 + 0.67(Ra_H \Psi)^{1/4}, & 10^5 < Ra_H < 10^9 \\ 0.15(Ra_H \Psi)^{1/3}, & 10^9 \le Ra_H < 10^{11} \end{cases} \tag{B8}$$

where $H_{l(v)}$ is the height of the liquid/vapor in contact with a vertical wall.

Appendix C: Model Parameters

Model parameter values are given in Table C1. Here, d_w refers to the tank wall thickness.

References

[1] Osipov, V. V., Daigle, M. J., Muratov, C. B., Foygel, M., Smelyanskiy, V. N., and Watson, M. D., "Dynamical Model of Rocket Propellant Loading with Liquid Hydrogen," *Journal of Spacecraft and Rockets*, Vol. 48, No. 6, Nov. 2011, pp. 987–998. doi: 10.2514/1.52587

[2] Daigle, M., Foygel, M., and Smelyanskiy, V., "Model-Based Diagnostics for Propellant Loading Systems," *2011 IEEE Aerospace Conference Proceedings*, IEEE Publ., Piscataway, NJ, March 2011.

[3] Lin, W., and Armfield, S. W., "Direct Simulation of Natural Convection Cooling in a Vertical Circular Cylinder," *International Journal of Heat and Mass Transfer*, Vol. 42, No. 22, Nov. 1999, pp. 4117–4130. doi: 10.1016/S0017-9310(99)00074-5

[4] Ho, S. H., and Rahman, M. M., "Transient Analysis of Cryogenic Liquid Hydrogen Storage Tank with Intermittent Forced Circulation," *Journal of Thermophysics and Heat Transfer*, Vol. 24, No. 2, 2010, pp. 374–380. doi:10.2514/1.41135

[5] Cheng, P., Zhao, T. S., and Pu, W. L., "An Experimental Study of Mixed Convection Heat Transfer in Vertical Packed Channels," *Journal of Thermophysics and Heat Transfer*, Vol. 13, No. 4, 1999, pp. 517–521. doi: 10.2514/2.6470

[6] Panzarella, C. H., and Kassemi, M., "On the Validity of Purely Thermodynamic Descriptions of Two-Phase Cryogenic Fluid Starage," *Journal of Fluid Mechanics*, Vol. 484, June 2003, pp. 41–68. doi:10.1017/S0022112003004002

[7] Schallhorn, P., Campbell, D. M., Chase, S., Puquero, J., Fontenberry, C., Li, X., and Grob, L., "Upper Stage Tank Thermodynamic Modelling Using SINDA/FLUINT," *44rd AIAA/ASME/SAE/ASEE Joint Propulsion Conference and Exhibit*, AIAA Paper 2006-5051, July 2006.

[8] Wang, Y. Z., Hua, Y. X., and Meng, H., "Numerical Studies of Supercritical Turbulent Convective Heat Transfer of Cryogenic-Propellant Methane," *Journal of Thermophysics and Heat Transfer*, Vol. 24, No. 3, 2010, pp. 490–500. doi: 10.2514/1.46769

[9] Barsi, S., Moder, J., and Kassemi, M., "Numerical Investigation of LO2 and LCH4 Storage Tanks on the Lunar Surface," *44rd AIAA/ASME/SAE/ASEE Joint Propulsion Conference and Exhibit*, AAIA Paper 2008-4749, 2008.

[10] Ahuja, V., Hosangadi, A., Mattick, S., and Lee, C. P., "Computational Analyses of Pressurization in Cryogenic Tanks," *44rd AIAA/ASME/*

SAE/ASEE Joint Propulsion Conference and Exhibit, AIAA Paper 2008-4752, 2008.s

[11] Khurana, T. K., Prasad, B. V. S. S. S., Ramamurthi, K., and Murthy, S. S., "Thermal Stratification in Ribbed Liquid Hydrogen Storage Tanks," *International Journal of Hydrogen Energy*, Vol. 31, No. 15, Dec. 2006, pp. 2299–2309. doi:10.1016/j.ijhydene.2006.02.032

[12] Moran, M. E., "Cryogenic Fluid Storage Technology Development: Recent and Planned Efforts at NASA," *JANNAF Spacecraft Propulsion Subcommittee (SPS) Meeting*, NASA Glenn Research Center, Cleveland, OH, 2008; also NASA TM-2009-215514, March 2009.

[13] Doherty, M. P., Gaby, J. D., Salerno, L. J., and Sutherlin, S. G., "Cryogenic Fluid Management Technology for Moon and Mars Mission," NASA TM-2010-216070, 2010; also AAIA Paper 2009-5632, 2009.

[14] Brennen, C. E., *Fundamentals of Multiphase Flow*, Cambridge Univ. Press, Pasadena, CA, 2005, p. 150.

[15] Schmidt, F. W., Henderson, R. E., and Wolgemuth, C. H., *Introduction to Thermal Sciences*, 2nd ed., Wiley, New York, 1993, pp. 101–179.

[16] Kakac, S., Shah, R. K., and Aung, W. (eds.), *Handbook of Single-Phase Convective Heat Transfer*, Wiley, New York, 1987, p. 12.1.

[17] von Karman, T., "On Laminar and Turbulent Friction," National Advisory Committee for Aeronautics TM 1092, Washington, DC, Sept. 1946.

[18] Eckert, E. R. G., and Jackson, T. W., "Analysis of Free-Convection Boundary Layer on Flat Plate," National Advisory Committee for Aeronautics TM 2207, Washington, DC, Sept. 1950.

[19] Yao, L. S., and Molla, M., "Non-Newtonian Fluid Flow on a Flat Plate Part 1: Boundary Layer," *Journal of Thermophysics and Heat Transfer*, Vol. 22, No. 4, 2008, pp. 758–761. doi: 10.2514/1.35187

[20] Yao, L. S., and Molla, M., "Non-Newtonian Fluid Flow on a Flat Plate Part 2: Heat Transfer," *Journal of Thermophysics and Heat Transfer*, Vol. 22, No. 4, 2008, pp. 762–765. doi: 10.2514/1.35190

[21] Schlichting, H., and Gersten, K., *Boundary-Layer Theory*, 8th ed., Springer, Berlin, 2000, p. 241.

[22] Landau, L. D., and Lifshitz, E. M., *Fluid Mechanics*, 2nd ed., Pergamon Press, Oxford, England, 1987, p. 361.